Title
A Comparison of Moored Acoustic Doppler Profiler Data and Satellite Altimeter Data on the Variability of East Greenland Current from 2016-2020

Permalink
https://escholarship.org/uc/item/7q26q0z2

Author
Yu, Aoming

Publication Date
2023

Peer reviewed|Thesis/dissertation

UNIVERSITY OF CALIFORNIA SAN DIEGO

A Comparison of Moored Acoustic Doppler Profiler Data and Satellite Altimeter Data on the Variability of East Greenland Current from 2016-2020

A thesis submitted in partial satisfaction of the
requirements for the degree Master of Science

in

Oceanography

by

Aoming Yu

Committee in charge:

 Fiammetta Straneo, Chair
 Janet Becker
 Janet Sprintall

2023

The Thesis of Aoming Yu is approved, and it is acceptable in quality and form for publication on microfilm and electronically.

University of California San Diego

2023

DEDICATION

I dedicate this thesis to my parents for their unwavering support, love, and encouragement throughout my academic pursuits. To my professors and peers who has guided and supported me to make me succeed. Without your support, this achievement would not have been possible.

TABLE OF CONTENTS

LIST OF FIGURES

ACKNOWLEDGEMENTS

ABSTRACT OF THE THESIS

A Comparison of Moored Acoustic Doppler Profiler Data and Satellite Altimeter Data on the Variability of East Greenland Current from 2016-2020

by

Aoming Yu

Master of Science in Oceanography

University of California San Diego, 2023

Fiammetta Straneo, Chair

The East Greenland Current (EGC) and the East Greenland Coastal Current (EGCC) are part of the North Atlantic Ocean circulation system that carries cold fresh melting water from the Arctic southward to the Subpolar North Atlantic region; hence, determining the variability and the drivers of these currents can help scientists to develop a better understanding of the circulation and climate in the Northern Hemisphere. In this study, we compare velocity from Acoustic Doppler Current Profilers (ADCP) data (2016-2020) from the Overturning in the Subpolar North Atlantic Program (OSNAP) moorings deployed near the Cape Farewell, at the

southern tip of Greenland, with the geostrophic velocity derived from satellite altimeter data from AVISO that measures the sea level anomalies (SLA). The goal is to determine which part of the moored observed variability can be derived from the altimeter data. It is found that the seasonal variability observed via the two methods is similar. Similarly, the magnitude of across flow velocity anomaly of the two data sets are the same, but the along flow velocity anomaly computed from the satellite altimeter data is slightly smaller than that of the mooring data. Overall, our results suggest that the satellite altimeter is a complementary tool for ocean circulation observation at high latitudes where moorings are not deployed.

Chapter 1

Introduction and Background

The East Greenland Current system mainly consists of the East Greenland Coastal Current (EGCC), which is a relatively narrow current carrying fresh, cold melting water from the Greenland glaciers and freshwater from the Arctic southward over the East Greenland continental shelf, and the East Greenland Current (EGC), which is a broader current that flows southward along the eastern coast of Greenland, carrying large volumes of Arctic water southward into the North Atlantic (Rudels et al., 2005). In addition, the EGC also interacts with other currents. Near the southeastern tip of Greenland, the EGC finally merges with warm and salty Irminger Current (IC) that originated from the North Atlantic Current (Lherminier et al., 2010), and flows around the southern tip of Greenland over the continental shelf break. In the region of the Labrador Sea, the EGC interacts with the Labrador Current and may affect the deep convection of the Labrador Sea Water, which can affect the Atlantic Meridional Overturning Circulation (AMOC) and global climate (Lavender et al., 2005, Yashayaev et al., 2017).

Despite its importance, the EGC is still not fully understood due to limited observations, and its variability and response to climate change remain an active area of research. In the past, data were limited to shipboard observations in the summer, and continuous year-round observations over the EGC system were not made until the Overturning in the Subpolar North Atlantic Program (OSNAP) observing system was launched. In the summer of 2014, a set of eight mooring arrays were deployed to the southeast of Greenland, extending from above the continental shelf to the slope southeast of Greenland at approximately 60°N (Holliday et al.,

2018; Li et al., 2017; Lozier et al., 2017). The eight moorings span about 100 km. The first two years of data (2014-2016) of the EGC system are described by Le Bras et al. (2018). The amount of freshwater transported by the EGCC and EGC reached a maximum in late fall and winter respectively, suggesting that the summer measurements made in the past underestimated the freshwater transport. By decomposing the coastal current freshwater transport variability, Le Bras et al. (2018) found that the variability in the current's velocity dominates the seasonality of freshwater transport instead of variability due to changes in salinity.

The OSNAP data up to 2020 is under investigation. To my knowledge, there has not been any research comparing the mooring data with geostrophic currents derived from satellite altimetry to investigate the EGC circulation. Thus, I extended the record to cover the 2014-2020 period and investigate the variability of EGC over the six-year record. The satellite altimetry data only covers the period from 2016-2020, so we focused on analyzing the mooring data from 2016-2020 for the comparison. This thesis aims to contribute to our understanding of the velocity of the EGC by investigating its interannual and seasonal variability using a combination of two observational approaches including moored Acoustic Doppler Current Profilers (ADCPs) and AVISO satellite altimetry. In addition, by comparing the two observational platforms, we want to investigate the usefulness of satellite altimetry in the Greenland region. If the results from the two data sets are mostly consistent, the implication is that the satellite altimetry can be used as a complementary tool for scientists to better study the EGC and ocean circulation in the high latitudes.

In this study, we used moored ADCP data from the EGC at the OSNAP transect and gridded AVISO satellite altimetry data that measures the sea level anomalies. We compare the anomaly of the EGC surface velocity with the geostrophic velocity anomaly computed from the

sea level anomaly data. We find that the satellite altimeter data can reproduce most of the current velocity anomaly as measured by moored ADCP. Since the spatial and time resolution of the satellite altimeter is 25 km/3 days, there are some limitations. The EGCC cannot be captured by the satellite altimetry since it is very narrow and flows along the East Greenland coast, hence, in this paper, we seek to investigate the variability of EGC. We set the time range of the ADCP data to be the same as the satellite data, and low-pass filter the ADCP data with a ten-day interval to match with the satellite data.

This paper is organized as follows. We describe the data and methods used in Chapter 2. The analysis procedures and comparison results computed from the ADCP data and satellite altimeter data are presented in Chapter 3. In Chapter 4, we discuss the context and implication of the EGC variability.
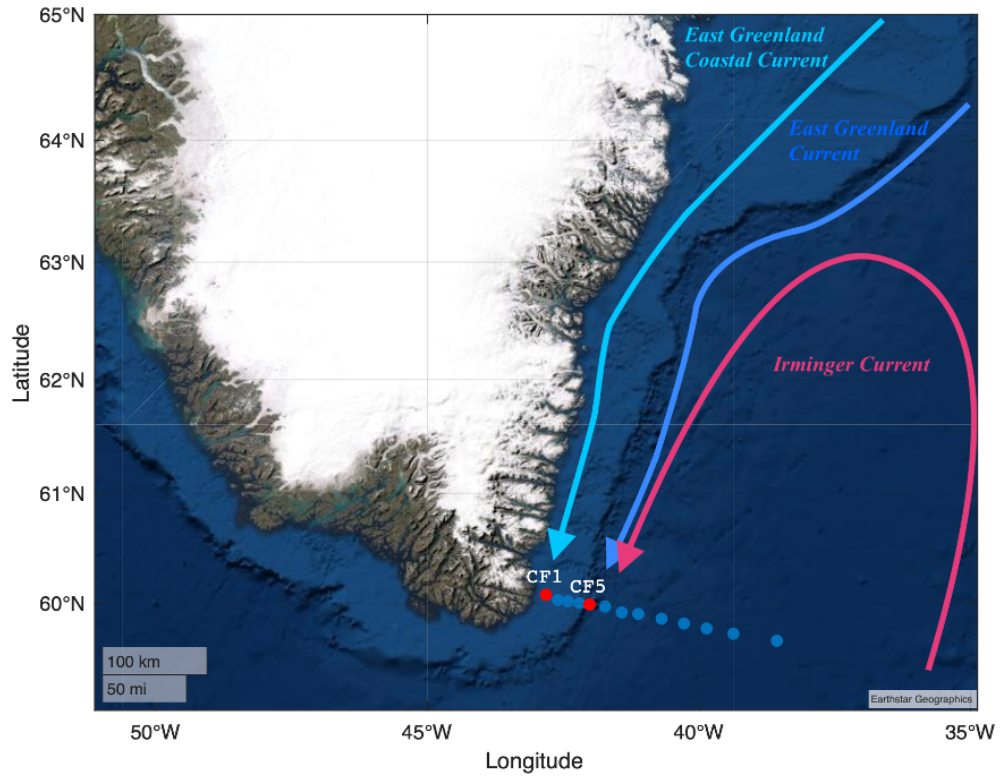
Figure 1.1. Map of study area with schematic arrows showing the approximate positions of the currents in the EGCC system and the position of the OSNAP moorings and OOI (Ocean Observatories Initiative) moorings along the OSNAP East line.

Chapter 2
Data and Methods

2.1 Data

In this section we introduce the data from two observational platforms that we analyzed to understand the variability of the EGC: moored ADCP data collected near Cape Farewell and data from satellite altimetry data over the North Atlantic region.

2.1.1 OSNAP Mooring

The East Greenland Continental shelf is a critical region for studying oceanic circulation and its associated dynamics. In 2014, the OSNAP observing system deployed a set of eight moorings along the OSNAP East line (from southeastern tip of Greenland to Scotland). The primary instruments we used are 75 kHz Acoustic Doppler Current Profilers (ADCPs) and point current meters attached to mooring CF1 to CF7, and M1. Velocity records were measured over a 6-hour interval. Raw velocity data was low-pass filtered with a 40-hour cutoff to remove tides. In addition, we use velocity data from all of the OSNAP East line moorings – which was gridded daily from 2014 to 2020 along the OSNAP East line, which spans 240 km. The data has also been linearly interpolated in depth between the surface and 3000m (depth at mooring CF5 is approximately 1250 m), with a spatial resolution of 10m. Figure 2.1 displays the time series of interpolated EGC velocity at various depths, measured at mooring CF5 (59.99°N, 42.02°W, marked by red dot in Figure 1.1). In this study, we showed the upper 20m mean current velocities passing the OSNAP transect with the gridded data. For the analysis of the EGC

velocity variability, we utilized the gridded data between mooring CF4 and CF6 since the EGC

passes the location of mooring CF5 approximately.
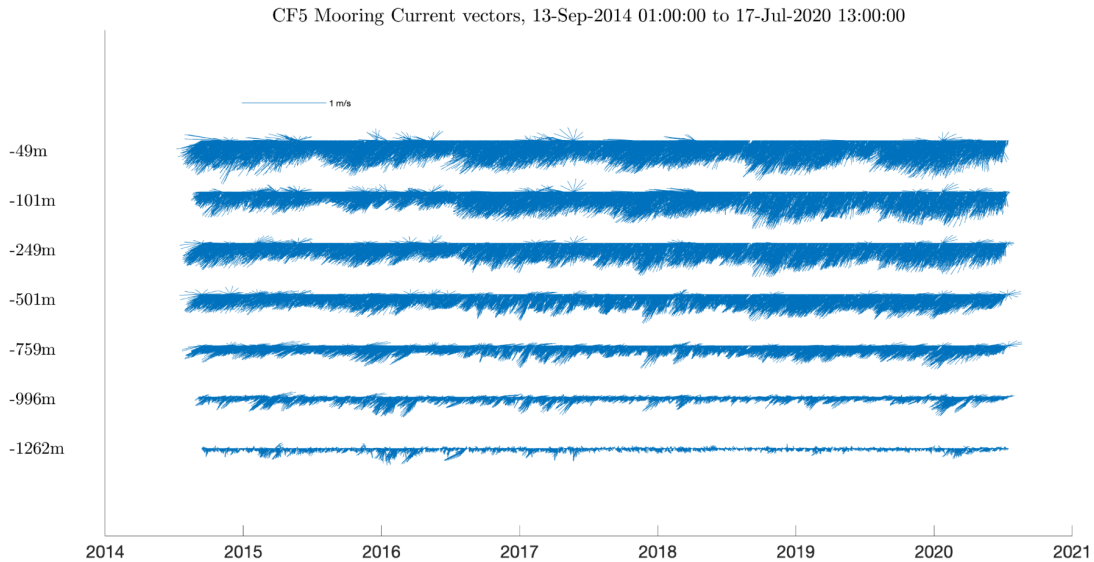
Figure 2.1. Stick plot of EGC's velocity vectors at different depths at mooring CF5 (59.99°N, 42.02°W) over the period from 13-Sep-2014 01:00:00 UTC to 17-Jul-2020 13:00:00 UTC.

2.1.2 Satellite Altimetry

For the satellite altimetry data, sea level anomalies computed with respect to a twenty-

year mean from Archiving, Validation, and Interpretation of Satellite Oceanographic data

(AVISO) product with processing by SSALTO/DUACS. Three satellites (Sentinel-3, Cryosat-2,

and SARAL/AltiKa) are used to generate sea level data, each producing a separate mono-mission

gridded products. These individual products then are combined using optimal interpolation to

create a multi-mission gridded product (Prandi et al., 2021). The data span from July 2016 to

June 2020, with a spatial resolution of 25 km and temporal resolution of 3 days. The data is

gridded in the format of EASE (The Equal-Area Scalable Earth) Grids 2.0, which are versatile

formats for global-scale gridded data, including remotely sensed data (described by Brodzik et al., 2012). We converted the geographic coordinates (longitude, latitude) to EASE(2)-grid coordinates (column, row) by using the python package ease_latlon. With the column and row numbers, we can obtain the sea level anomalies (SLA) at the desired latitude and longitude.

The mean SLA of 2016-2020 is presented in Figure 2.2. The Irminger basin and the region close to the continental shelf in the East Greenland Sea exhibit mostly negative SLA. The standard deviation of the SLA is shown as the contour lines. Near the East Greenland southeast coast, the contour lines are tightly spaced, indicating a higher variability in the SLA. This suggests that the sea level in the area nearby the East Greenland southeast coast experiences relatively more rapid changes over time compared to other regions.
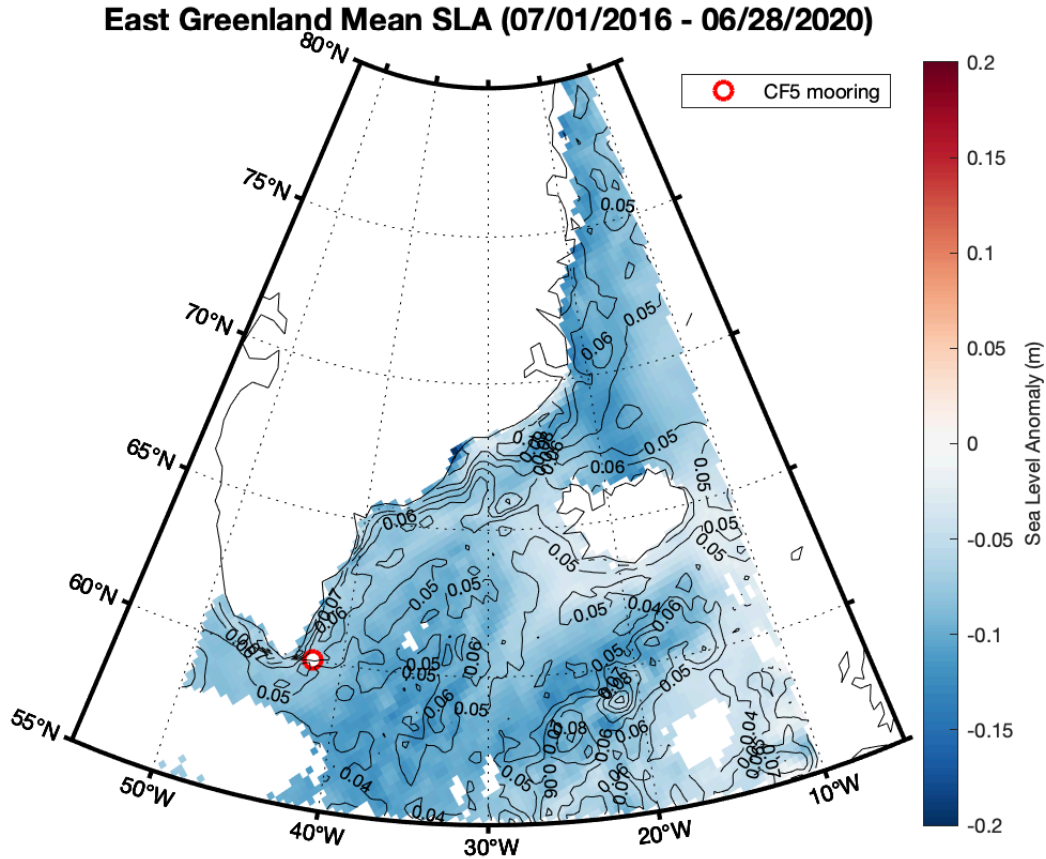
Figure 2.2. Time-mean SLA (7/1/2016-6/28/2020), with the standard deviation overlaid in contours. Red dot shows the OSNAP CF5 mooring location.

2.2   Methods

The purpose of this study is to compare the velocity derived from moored ADCPs with satellite altimeter data, so we need to average the satellite data in time and space so it has similar resolution as the mooring data. The gridded ADCP data gives us the absolute current velocity at 1 day resolution, while the satellite altimeter data gives us the sea level anomalies (SLA). The twenty-year mean sea surface height that was used to compute the SLA is unknown because the earth's geoid is not known, so we can only compare the current velocity anomaly from the

ADCP data with the geostrophic velocity anomaly derived from the SLA. The methods

employed in this paper are described below.

2.2.1 Current Velocity Anomaly

Mean across flow velocity and along flow velocity of the upper 20 m of depth at mooring

location CF5 is calculated by averaging the daily gridded velocities between mooring CF4

(mooring to the west of CF5) and CF6 (mooring to the east of CF5) from 2014-2020. Here we

computed the velocity mean using the original full data record (2014-2020), then subtract the

mean from absolute velocity to get the anomalies from 2014-2020. We cut off the anomalies

from 2014-2016 to match with the time range of satellite altimeter data (2016-2020). Since the

mooring data has a time resolution of one day, it needs to be subsampled on approximately the

same time grid as the altimeter data. We applied a running mean to smooth the satellite altimeter

data by convolving the data as follows. The basic convolution integral is:

$$y(t) = \int_{-\infty}^{\infty} h(\tau)x(t-\tau)d\tau$$

where x is the data and h is a filtering operator.

The mooring data has a time resolution of 1 day while the satellite altimeter data has a

time resolution of 3 day. In this study, we use a "boxcar" filter to get a 10-day running mean of

mooring data to make the temporal and spatial resolution of the two data sets have similar

magnitude.

2.2.2 Geostrophic Velocity Anomaly

The satellite altimetry data gives us the sea level anomalies with respect to a twenty-year mean, so we can compute surface geostrophic velocities using the following geostrophic balance:

$$u_g = -\frac{g}{f}\frac{\partial \zeta}{\partial y}$$

$$v_g = \frac{g}{f}\frac{\partial \zeta}{\partial x}$$

where (u_g, v_g) is the surface geostrophic velocity, g is Earth's gravity, $f = 2\Omega \sin\theta$ is the Coriolis parameter (with $\Omega = 7.29 \cdot 10^{-5} s^{-1}$), and ζ is the sea surface height.

Here we capture a 20 by 20 grid of sea level anomalies (SLA) data, with longitude ranging from 35°W to 44.5°W and latitude ranging from 59°N to 60°N to cover the region in which the OSNAP moorings were deployed in. By using a center differencing technique, we compute the surface geostrophic velocity anomaly at a fixed location with the SLA and distance difference between the right and left (north and south) end of that fixed location. $\partial\zeta$ is calculated directly by subtracting the SLA values of the two edges of each grid box. ∂x and ∂y are calculated using the following equations:

$$\partial x = (\lambda_{east} - \lambda_{west}) * R * \cos\theta * \frac{\pi}{180°}$$

$$\partial y = (\theta_{north} - \theta_{south}) * R * \frac{\pi}{180°}$$

where λ_{east} and λ_{west} are the longitudes of the east and west end of the fixed location, θ_{north} and θ_{south} are the latitudes of the north and south end of the location, and R is Earth's radius (approximately 6,400,000 m).

2.2.3 Interpolation and Rotation

After computing the geostrophic velocity anomalies within the 20° by 20° spatial grid, we interpolated the geostrophic velocity anomalies onto the OSNAP East line. The OSNAP East line was linearly interpolated to 121 points, with the west end at 60.08°N, 42.817°W and east end at 59.6572°N, 38.5999°W. With interpolation, we get a rough estimation of the geostrophic velocity anomalies of current through the OSNAP East line. We are interested in the surface geostrophic velocity anomaly of the EGC, which is at the location of CF5 mooring, so we averaged the geostrophic velocity anomalies over the 15 points between CF4 mooring (west side of CF5) and CF6 mooring (east side of CF5) to get a more precise result that can be compared with the mooring data anomaly.

In addition, we performed a rotation after interpolating the geostrophic velocity anomalies onto the OSNAP transect. The along-stream flow derived from the mooring is 214° from the north. This angle is the principle axis of the EGC, located at the center of the slope current, which is similar to the angle of 203.3° used by Le Bras et al (2018). The unrotated geostrophic velocity anomaly v_g is to the south (180° from north), so we rotated the surface geostrophic velocity anomaly by 34° clockwise to derive the along flow velocity anomaly.

Chapter 3

Results

This section presents an analysis of the variability exhibited by the currents traversing the OSNAP transect. Firstly, we examine the interannual variability of the surface East Greenland Current (EGC) as measured by the deployed moorings. Subsequently, we investigate the seasonal variability of surface geostrophic velocity anomaly associated with the EGC. Furthermore, we provide a comparative analysis of the velocity anomaly of the EGC and the surface geostrophic velocity anomaly derived from the satellite data.

3.1 Variability of Currents Traversing the OSNAP Transect

The eight moorings deployed along the OSNAP East line provide insight into the absolute velocity of the EGCC (at CF1) and EGC (at CF5), which flows the fastest compared to the currents passes the other moorings along the transect and transports the largest volume amount of fresh cold water southward along the shelf and over the continental slope. By conducting a freshwater transport analysis, Le Bras et al. (2018) found that EGC and EGCC have staggered seasonality, with the peak of EGCC occurring in late fall, preceding the peak of EGC during the winter. With the moored ADCP data from 2014-2020, we present the seasonal and annual mean velocity of currents in the upper 20 meter that passes the OSNAP East line transect (Figure 3.1). Our result shows two velocity peaks, EGCC at the coast (0 km) and EGC at 46 km from the coast, which conforms with our expectation. We observe that EGCC velocity peak happens in fall (Sep, Oct, Nov) and EGC has a velocity peak in winter (Dec, Jan, Feb). Le Bras'

transport analysis used the data from 2014-2016, she found that during 2014-2015 the EGCC transport peaks in December, which is earlier than EGC's transport peak in March. In 2015-2016, however, the peaks of EGC and EGCC transport happened earlier during 2015-2016, with the EGCC peaking in October and EGC peaking in December. Our result of the current velocity in the upper 20 meter also provides additional evidence for the seasonal pattern of freshwater transport. The EGCC exhibits the highest velocity and experiences a peak in freshwater transport during the fall, whereas the EGC demonstrates these characteristics during winter. Furthermore, it is worth noting that the currents traversing the transect exhibit their minimum velocities during the summer. This observation agrees with the seasonality described by Le Bras et al. (2018), which implies that previous measurements pertaining to freshwater transport and current velocities were likely underestimated, given that the measurements were solely conducted during the summer.

While our study primarily examines data from 2016 to 2020, we conducted a comparison of the annual mean velocity of the currents traversing the OSNAP transect for each year. Our findings indicate that the annual mean velocity of the EGC is approximately -0.6188 ± 0.0118 m/s over the period from 2016-2020. This velocity is higher than the approximate value of -0.5330 ± 0.0043 m/s observed during 2014-2016 (Figure 3.1b). The drivers of the velocity difference may be due to changes in water temperature in the East Greenland region, which cause an increase in freshwater transport, or it could be due to changes in wind patterns. Future work can be conducted to determine the drivers that have influenced the observed change in EGC velocity since 2016.
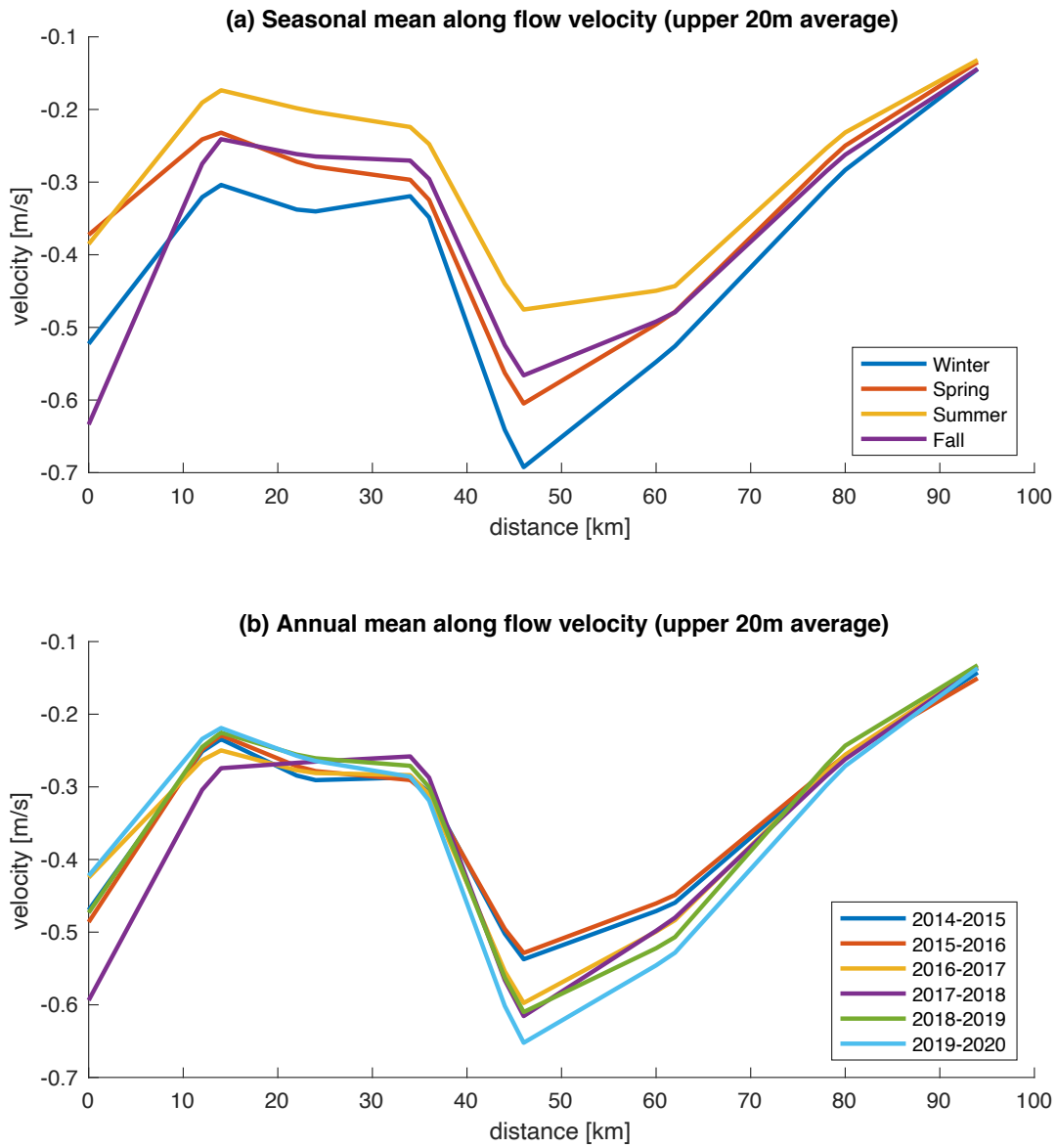
Figure 3.1. (a) Seasonal mean velocity of along flow traversing the OSNAP transect, (b) Annual mean velocity of along flow traversing the OSNAP transect. Both were averaged over the upper 20 meters.

3.2 EGC Velocity Interannual Variability

To investigate the variability of EGC traversing the mooring CF5, we computed the monthly mean of the upper 20m mean of across flow velocity and along flow velocity velocities measured by mooring CF5 (Figure 3.2). Throughout the time series, both across flow velocities and along flow velocities exhibit negative values, indicating a consistent southwestward flow. However, the across flow velocity alone does not capture the seasonal trend effectively, as it can oscillate eastward or westward due to wind events or oceanic circulation. In contrast, the along flow velocity displayed a distinct seasonal pattern in the time series. The EGC's velocity reached a minimum (less negative) during the summer months (mainly August and September), followed by a rapid increase (more negative) in the late fall and subsequent maxima either in December or January. Subsequently, the velocity began to increase during late winter and spring. Within the spring season, the monthly mean velocity of the upper 20 meters mean across flow velocity exhibited more oscillations than along flow velocity. Further research is needed to understand the driving mechanisms behind the observed oscillations and their impact on the behavior of the EGC during different seasons.
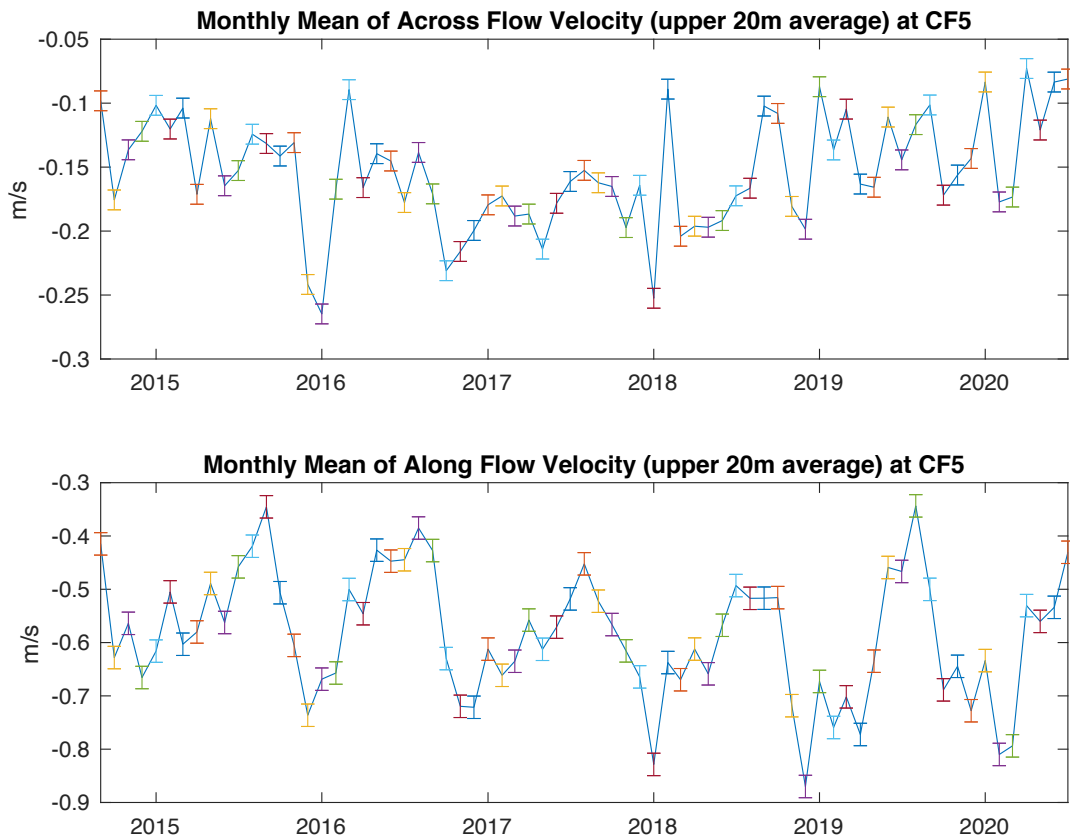
Figure 3.2. Monthly mean of across flow velocity and along flow velocity of EGC at mooring CF5, with red bars showing the standard deviations.

3.3 Sea Level Anomaly Interannual Variability

We utilized sea level anomaly (SLA) data from the East Greenland region to perform interpolation onto the OSNAP transect. Our objective was to examine SLA variations across different locations along the transect line over multiple years, which led us to generate a Hovmoller plot. The plot clearly illustrates an upward trend in SLA from 2016 to 2020. In 2020, the SLA near the East Greenland Coastal Current (EGCC) exhibited relatively higher values (> 0.05m) compared to previous years, as indicated by a darker shade of red. Furthermore, during the 2019-2020 cycle, the SLA showed increased values during the summer and fall. By visually

analyzing Figure 3.3, it can be observed that the maximum SLA peaks typically occur in late fall, while the minimum values are observed during mid-winter. The SLA near the coast exhibits a slight elevation compared to offshore areas. Overall, we observe a relatively consistent seasonality of SLA across various locations along the transect.
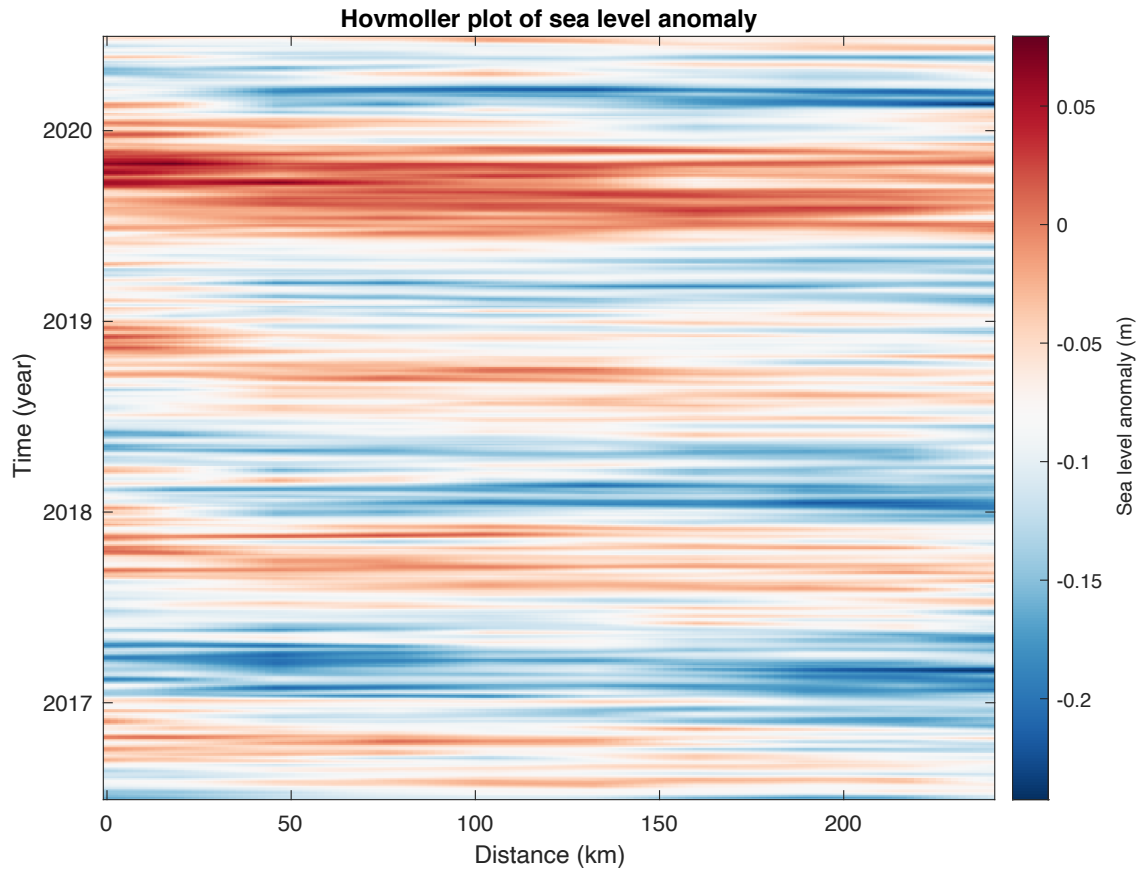

Figure 3.3. Hovmoller plot of SLA at different locations along the OSNAP transect.

3.4   Seasonality of Geostrophic Velocity Anomaly

To gain a comprehensive understanding of the ocean circulation in the East Greenland region, we constructed geostrophic velocity anomaly plots incorporating sea level anomalies (SLA) as the background. The SLA representation utilized a 50 by 50 grid, with the across flow and along flow of the geostrophic currents depicted as vector arrows. Notably, a significant contrast in SLA was observed between the vicinity of the Kangerlussuaq Fjord of East Greenland (68.43° N, 32.55°W) and the offshore regions, as evident from the winter and summer maps of geostrophic velocity anomaly (Figure 3.4). The maps offer insights into the spatial distribution of geostrophic velocity anomaly. In accordance with the geostrophic balance, the Coriolis force and the pressure gradient force maintain equilibrium. In the northern hemisphere, high pressure (high SLA) is to the right of the geostrophic flow, while low pressure is to the left of the flow. We can observe that the EGC exhibits the largest geostrophic velocity anomaly over the slope southeast of Greenland and when traversing the Denmark Strait. During winter, the geostrophic velocity anomaly's direction is southwestward, while during summer, the direction is northeastward. The maps align with our previous findings, indicating that the velocity of the EGC reaches its peak during winter and reaches a minimum during summer.
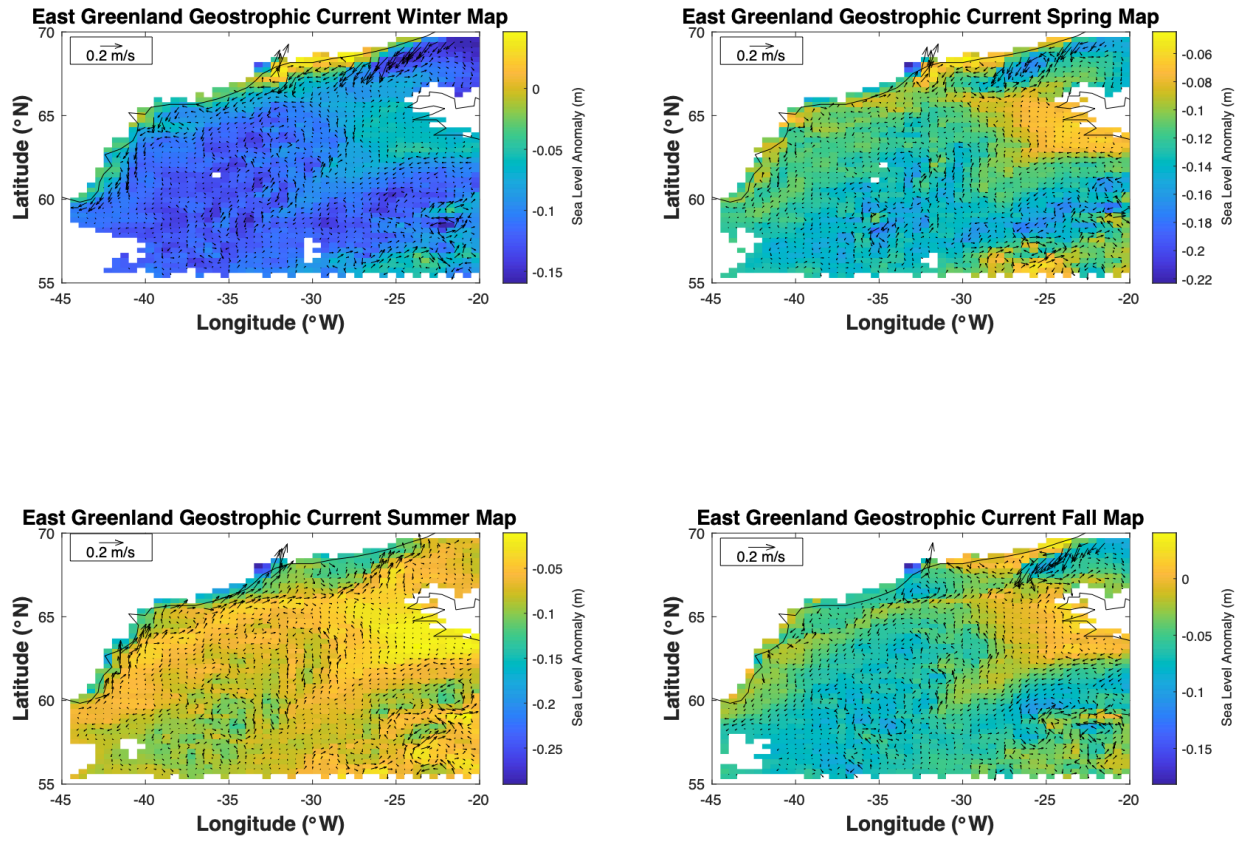
Figure 3.4. Seasonal maps of the East Greenland sea level anomaly and geostrophic velocity anomaly, averaged over the period from 2016 to 2020.

3.5 Comparison Result

The time series analysis of the across flow velocity anomalies and along flow velocity anomalies from the moored ADCP current velocity anomaly data and the geostrophic velocity anomalies reveals a correspondence and agreement between the two datasets. Specifically, the across flow velocity anomalies show a high degree of similarity. In terms of the along flow velocity anomalies in both data sets, they both display a seasonal pattern, suggesting a recurring variability in the north-south current velocity. However, the along flow of the geostrophic velocity anomaly data exhibits a smaller amplitude compared to the current velocity anomaly computed from the mooring data. The observed discrepancy may be due to ageostrophic velocities observed by moorings, which the satellite data does not resolve. This indicates that the geostrophic velocity is not the dominant component of the direct flow. Consequently, the geostrophic velocity anomalies calculated from satellite altimetry data exhibits a diminished magnitude when compared to the directly measured current velocity anomalies obtained from the moored ADCP data (Figure 3.5b). To compute the correlation coefficient (r) between the two datasets, the satellite data is interpolated to have the same timestamp as the mooring data. For the across flow velocity anomalies, r is approximately 0.32. For the along flow velocity anomalies, r is approximately 0.63. These results indicate that the mooring along flow velocity anomalies have a relatively strong correlation with the altimeter along flow velocity anomalies. After applying a 20-point (60-days, satellite data has a temporal resolution 3 days) moving average filter, we observe that smoothed across flow velocity anomalies of the two datasets have similar magnitude. The altimeter anomalies exhibit a slight seasonal pattern. For the along flow velocity anomalies comparison, the smoothed anomalies of both datasets display a seasonal pattern. The

most negative anomalies occur in winter, while the most positive anomalies are observed in late summer and early fall.

The stick plots (Figure 3.6) help us to compare the current velocity anomaly and geostrophic velocity anomaly more easily. These plots reveal variations in anomalies across different seasons, highlighting the distribution between positive and negative values. Negative anomalies are primarily observed during fall and winter, while positive anomalies are more prevalent in late spring and summer. Both stick plots in Figure 3.6 have a scale of 0.1 m/s, but the length of scale bars are not the same since they depend on the magnitude of each dataset's anomalies respectively. Therefore, if the vector scale lengths were the same for both plots, the vector sticks in the OSNAP mooring data plot would appear longer than they currently appear since the scale bar is shorter compared to that of satellite altimeter plot. A significant difference can be observed in terms of magnitude, especially regarding the positive anomalies. The positive anomaly magnitude for geostrophic velocity is lower than that of the current velocity anomaly during the summer of 2019, representing the most pronounced disparity between the two datasets. Overall, the comparison of the two datasets demonstrates similarities in the directional patterns of the anomalies and their seasonal variations, implying that the satellite altimeter is a complementary tool to study the ocean circulation in high latitudes.

(a) Across-flow velocity anomalies comparsion

Legend:
- Mooring Across
- Altimeter Across
- Mooring Across 20-points moving average
- Altimeter Across 20-points (60days) moving average

(b) Along-flow velocity anomalies comparsion

Legend:
- Mooring Along
- Altimeter Along
- Mooring Along 20-points moving average
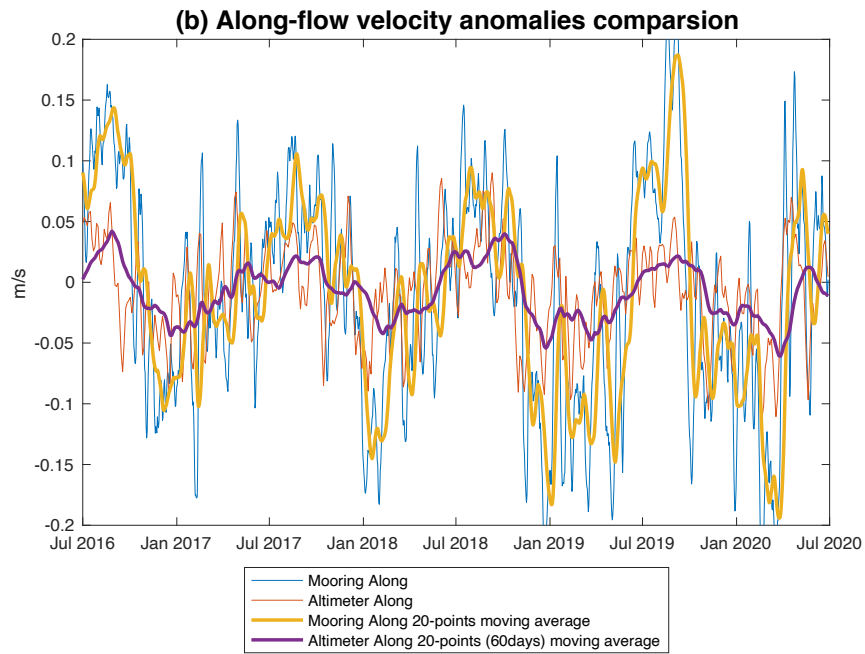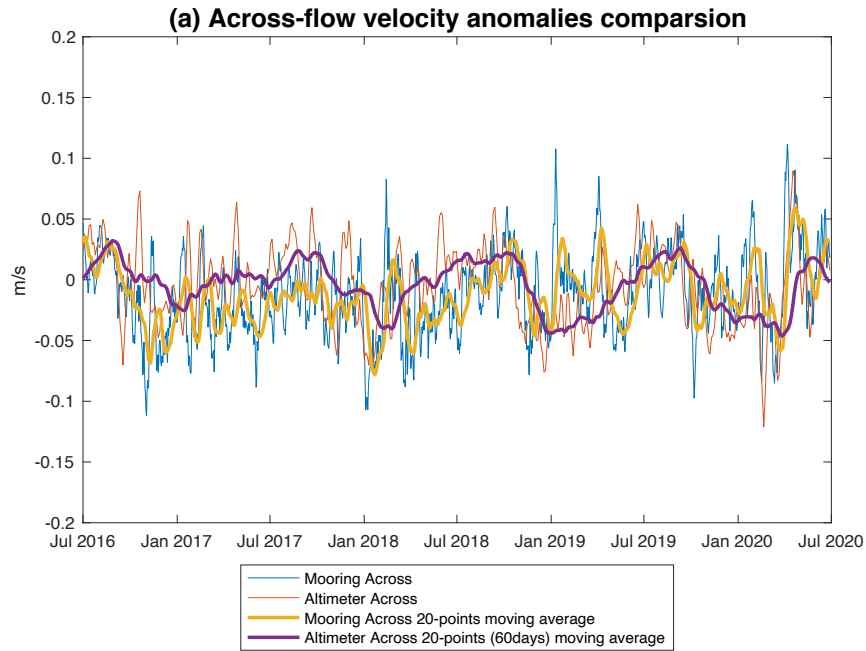- Altimeter Along 20-points (60days) moving average

Figure 3.5. Comparison of time series between current velocity anomaly and geostrophic velocity anomaly. (a) across flow velocity anomalies comparison, (b) along flow velocity anomalies comparison.
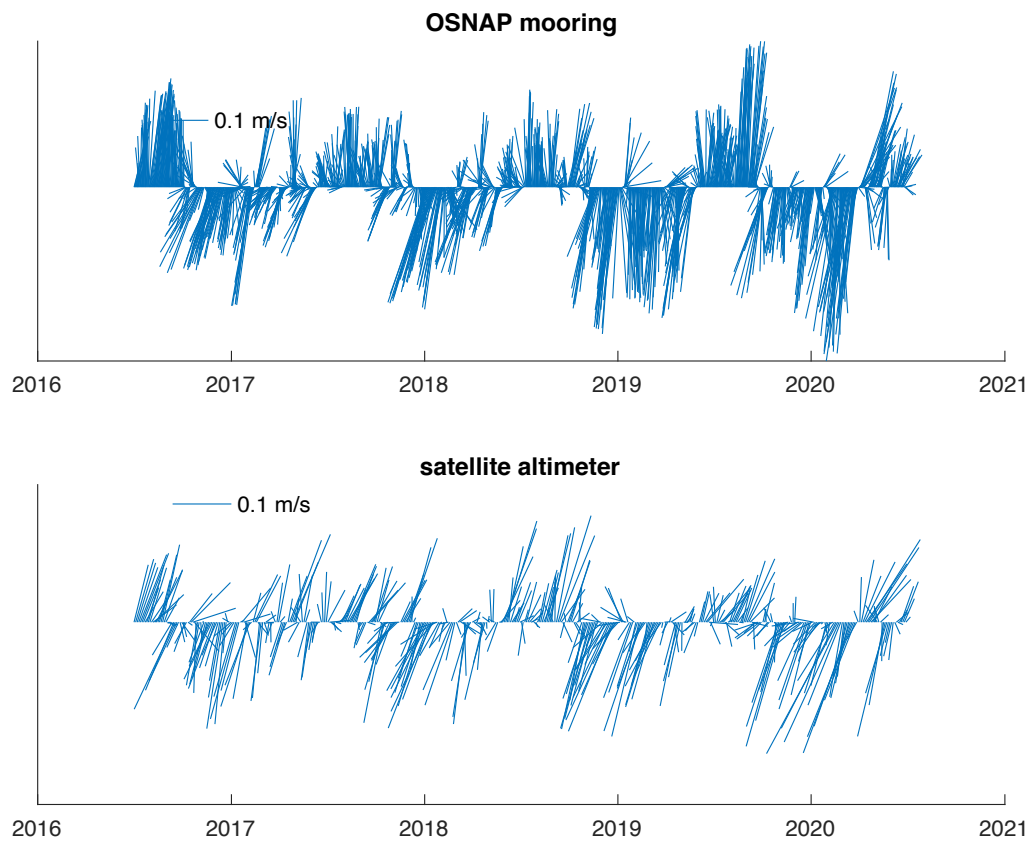
Figure 3.6. Stick plots of current velocity anomaly (upper panel) and geostrophic velocity anomaly (lower panel).

Chapter 4

Discussion

Using data from the OSNAP moorings, we examined the variability of the EGC. An ADCP accurately measures the velocity of the current that passes through the region covered by moorings and captures the large-scale ocean circulation very well. Satellite altimetry, on the other hand, provides larger spatial coverage. In this study, we compared moored ADCP data with estimated geostrophic currents from satellite altimeter data to investigate the variability of the EGC. Our findings show that the EGC velocity anomaly and geostrophic velocity anomaly, derived from the two datasets respectively, exhibits similar magnitude and direction over time. This highlights the complementary nature of satellite altimeter data in investigating surface geostrophic velocity in high latitudes.

Since the deployment of OSNAP moorings in 2014, no previous study has investigated the variability of EGC velocity using moored ADCP data from 2016-2020. Initially, we aimed to examine the variability of the East Greenland Coastal Current (EGCC), a southward flowing jet along the shelf of East Greenland determined by Bacon et al. (2002). However, due to the proximity of the mooring to the coast, SLA data for EGCC could not be captured by satellites. The EGC, located approximately 46 km from the coast, allowed for the capture of SLA data by the satellite altimeter. The velocity of the current has been shown to be highly correlated with freshwater transport, where higher velocity indicates a greater volume of freshwater being transported, as the area through which the freshwater passes remains constant (Le Bras et al. 2018). The EGC velocity results for the upper 20m align with the seasonal freshwater transport

analyzed by Le Bras et al. (2018), who categorized the EGC as water fresher than the reference salinity of 34.9, considering all fresh currents traversing the transect rather than a single location's velocity. Freshwater transport is given by:

$$\iint v(x,z)\rho(1-s)dxdz,$$

where v, ρ and s are along flow velocity (m/s), density (kg/m^3), and salinity (kg/kg) in full mks units. Here we did not compute the freshwater transport, but in a future study, one can compute the EGC freshwater transport passing through the vertical area between mooring CF4 and CF6 using full-depth velocity data and salinity data to roughly compare with Le Bras et al. (2018)'s results.

The results surpassed our initial expectations as our hypothesis was that the satellite altimeter, with its resolution of 3 days/25 km, is able to capture much of the velocity changes in the OSNAP transect region with relatively high precision. This comparison between the current velocity anomaly and the geostrophic velocity anomaly highlights the suitability of satellite altimetry for monitoring variations in ocean circulation in high latitudes. The SLA data allowed us to derive geostrophic velocity anomalies. However, without knowledge of the mean dynamic topography, we cannot directly obtain a comprehensive understanding of ocean circulation in the East Greenland region. To achieve this, it would be beneficial to combine SLA with the mean dynamic topography derived from AVISO's twenty-year data, resulting in absolute dynamic ocean topography.

Our study presents significant findings regarding the interannual and seasonal variability of the EGC velocity anomaly. These results hold reference value for further research on freshwater transport within the East Greenland region. Moreover, our study establishes the reliability of satellite altimeter data in computing geostrophic velocity anomalies of the currents

within this area. It is important to note that the application of satellite altimeter data extends

beyond the East Greenland region, enabling the study of surface geostrophic velocity anomalies

in other high latitude areas. Furthermore, our seasonal maps of SLA and geostrophic velocity

anomaly suggests that satellite altimeter data can be employed to investigate mesoscale cyclonic

eddies over the slope of the East Greenland continental shelf.

Appendix A

SLA Annual and Seasonal Mean Maps

We analyzed the changes in SLA over the years by calculating the annual mean SLA for each year (Figure A.1). We then calculated the SLA annual anomaly by subtracting the all-time mean SLA (2016-2020) from each year's data (Figure A.2). The SLA annual mean anomaly shows a shift from predominantly negative values in 2016 to predominantly positive values in 2020, indicating an increasing trend in SLA over time. The factors that contribute to the increase in SLA are not fully understood due to the complicated ocean dynamics in the region.
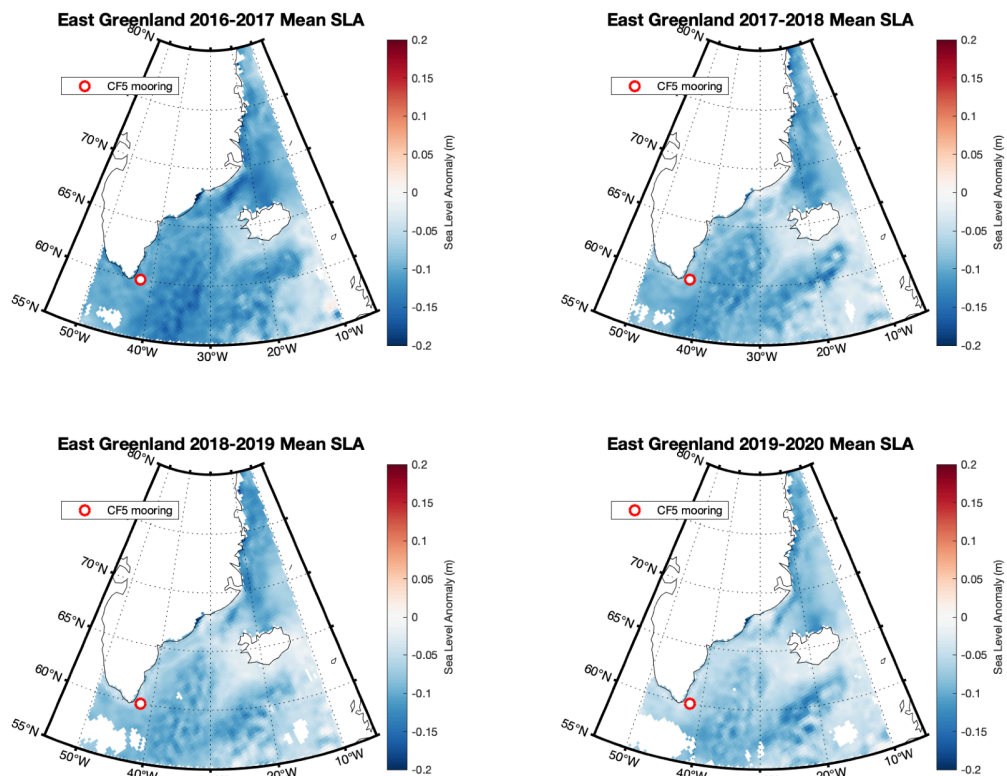

Figure A.1. The annual mean SLA for each year (16/17; 17/18; 18/19; 19/20)
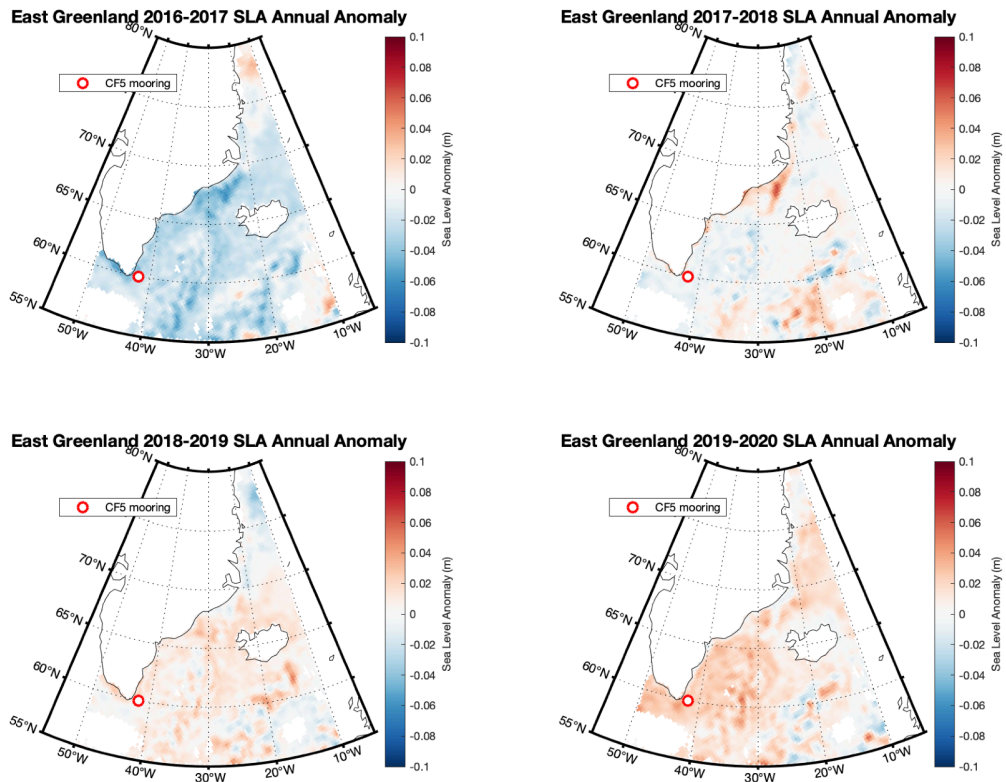
Figure A.2. The SLA annual anomaly for each year, using the time mean SLA

Since the satellite altimeter data covers the period from 7/1/2016 to 6/28/2020, there are a total of four summer seasons. However, it is important to note that 2016 and 2020 summer only provide two months of data, while the remaining three seasons consist of three years' worth of data (2016-2019 fall, 2016-2019 winter, 2017-2020 spring). The seasonal mean sea level anomaly (SLA) maps (Figure A.3.) clearly exhibits a contrast between different seasons. Specifically, in winter and spring, the SLA in the Irminger Sea and Greenland Sea regions is mostly negative. On the other hand, in summer and fall, the SLA in these regions is not as low compared to the other two seasons.

At 67°N 30°W, the SLA demonstrates a positive deviation in winter and a pronounced negative deviation in summer. When examining the winter and summer maps, a distinct observation can be made regarding the SLA on the East Greenland shelf. In winter, the SLA is higher in offshore region, while in summer, the pattern is reversed, with the SLA on the East Greenland Shelf being lower than the offshore SLA. The contrast is evident in the surrounding region of the Kangerlussuaq fjord in East Greenland when comparing the winter and summer maps. Bulczak et al. (2015) proposed a hypothesis suggesting that the increase in SLA during winter is attributed to wind-forced downwelling. Further investigation into coastal dynamics in the region can be conducted for future research.
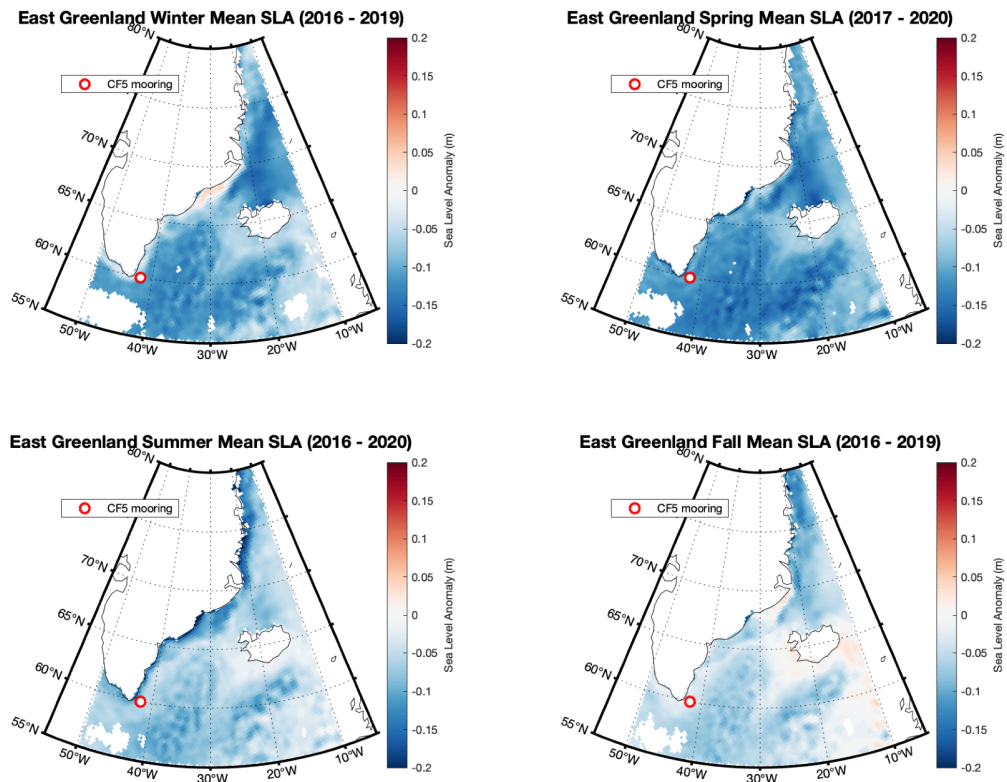

Figure A.3. Seasonal mean SLA (DJF; MAM; JJA; SON)

Bibliography

Brodzik, M. J., B. Billingsley, T. Haran, B. Raup, M. H. Savoie. (2012). EASE-Grid 2.0: Incremental but Significant Improvements for Earth-Gridded Data Sets. *ISPRS International Journal of Geo-Information*, 1(1):32-45, doi:10.3390/ijgi1010032.

Rudels, B., Björk, G., Nilsson, J., Winsor, P., Lake, I., & Nohr, C. (2005). The interaction between waters from the Arctic Ocean and the Nordic Seas north of Fram Strait and along the East Greenland Current: Results from the Arctic Ocean-02 Oden expedition. *Journal of Marine Systems*, 55, 1– 30.

Lherminier, P., Mercier, H., Huck, T., Gourcuff, C., Perez, F. F., Morin, P., Sarafanov, A., & Falina, A. (2010). The Atlantic Meridional Overturning Circulation and the subpolar gyre observed at the A25-OVIDE section in June 2002 and 2004. *Deep Sea Research Part I: Oceanographic Research Papers*, 57, 1374– 1391.

Lavender, K.L., Owens, W.B., Davis, R.E. (2005). The mid-depth circulation of the subpolar North Atlantic Ocean as measured by subsurface floats. Deep-Sea Res. I 52 (5), 767–785. http://dx.doi.org/10.1016/j.dsr.2004.12.007

Yashayaev, I., and Loder, J. W. (2017). Further intensification of deep convection in the Labrador Sea in 2016, *Geophys. Res. Lett.*, 44, 1429– 1438, doi:10.1002/2016GL071668.

Holliday, N. P., Bacon, S., Cunningham, S. A., Gary, S. F., Karstensen, J., King, B. A., Li, F., & Mcdonagh, E. L. (2018). Subpolar North Atlantic overturning and gyre-scale circulation in the summers of 2014 and 2016. *Journal of Geophysical Research: Oceans*, 123, 4538– 4559. https://doi.org/10.1029/2018JC013841

Li, F., Lozier, M. S., & Johns, W. E. (2017). Calculating the meridional volume, heat, and freshwater transports from an observing system in the subpolar North Atlantic: Observing system simulation experiment. *Journal of Atmospheric and Oceanic Technology*, 34, 1483– 1500.

Lozier, M. S., Bacon, S., Bower, A. S., Cunningham, S. A., Femke de Jong, M., de Steur, L., DeYoung, B., Fischer, J., Gary, S. F., Greenan, B. J. W., Heimbach, P., Holliday, N. P., Houpert, L., Inall, M. E., Johns, W. E., Johnson, H. L., Karstensen, J., Li, F., Lin, X., Mackay, N., Marshall, D. P., Mercier, H., Myers, P. G., Pickart, R. S., Pillar, H. R., Straneo, F., Thierry, V., Weller, R. A., Williams, R. G., Wilson, C., Yang, J., Zhao, J., Zika, J. D., Lozier, M. S., Bacon, S., Bower, A. S., Cunningham, S. A., de Jong, M. F., de Steur, L., DeYoung, B., Fischer, J., Gary, S. F., Greenan, B. J. W., Heimbach, P., Holliday, N. P., Houpert, L., Inall, M. E., Johns, W. E., Johnson, H. L., Karstensen, J., Li, F., Lin, X., Mackay, N., Marshall, D. P., Mercier, H., Myers, P. G., Pickart, R. S., Pillar, H. R., Straneo, F., Thierry, V., Weller, R. A., Williams, R. G., Wilson, C., Yang, J., Zhao, J., & Zika, J. D. (2017). Overturning in the subpolar North Atlantic Program: A new international ocean observing system. *Bulletin of the American Meteorological Society*, 98, 737– 752.

Le Bras, I. A.-A., Straneo, F., Holte, J., & Holliday, N. P. (2018). Seasonality of freshwater in the East Greenland Current system from 2014 to 2016. *Journal of Geophysical Research: Oceans*, 123, 8828– 8848. https://doi.org/10.1029/2018JC014511

Bulczak, A. I., Bacon, S., Naveira Garabato, A. C., Ridout, A., Sonnewald, M. J. P., and Laxon, S. W. (2015), Seasonal variability of sea surface height in the coastal waters and deep basins of the Nordic Seas, *Geophys. Res. Lett.*, 42, 113– 120, doi:10.1002/2014GL061796.

Prandi Pierre, Jean-Christophe Poisson, Yannice Faugère, Amandine Guillot, Gérald Dibarboure, (2021). Arctic sea surface height maps from multi-altimeter combination, Earth System Science Data, 10.5194/essd-13-5469-2021, 13, 12, (5469-5482).